Electrochemistry Communications 136 (2022) 107225

Contents lists available at ScienceDirect

Electrochemistry Communications

journal homepage: www.elsevier.com/locate/elecom

# Review of DFT-simulated and experimental electrochemistry properties of the polypyridyl Row-1 Mn, Fe & Co, and Group-8 Fe, Ru and Os MLCT complexes

Karel G. von Eschwege [2,*], Jeanet Conradie [1]

*Department of Chemistry, PO Box 339, University of the Free State, Bloemfontein 9300, South Africa*

ARTICLE INFO

*Keywords:*
DFT
Photocatalyst
MLCT
Cyclic voltammetry
Spectrum

ABSTRACT

Ruthenium had up to date been pivotal in electro- and photocatalytic applications involving reduction of $CO_2$ and $H_2O$, and dye-sensitized solar cells. Commercial applications would seek use of earth-abundant metals instead. Towards this goal, it is key to review the synthesis, electrochemical and spectroscopical properties of associated metal-to-ligand charge transfer complexes of row-4 (Mn, Fe & Co) and column-8 (Fe, Ru & Os). The present report is limited to data obtained under exactly similar conditions, providing scientifically valid correlations. Only *tris*-coordinated bipyridyl and phenanthroline complex derivatives are considered, being representative of catalysts and dyes traditionally used in the above-mentioned fields. The accuracy of theoretical DFT techniques to simulate complex properties is highlighted.

## 1. Introduction

In 2009 Gray expressed the need to replace fossil fuels by solar fuels [1]. These however, require chemical catalysts that are superior to what is presently available. Apart from high efficiency, increased stability, and of course, lower cost, are some of the demands. Ten years later Wenger asked: "Is iron the new ruthenium?" [2]. He mentioned that up to date ruthenium polypyridine complexes had been popular for applications in photophysics and photochemistry (eg. lighting, sensing, solar cells [3,4], electrocatalysis [5] and photoredox catalysis [6]), but that earth-abundant alternatives need to be found. Such a candidate may be iron. The challenge lies in the difference between the chemical structures of Fe and Ru, the latter allowing for long-lived photo-excited states (100 to 1000 ns) with charge-transfer readily taking place between the Ru metal and its ligands. In related iron metal-to-ligand charge transfer (MLCT) complexes the excited states are extremely short-lived, i.e. *ca* 50 fs, which is by far too short for useful applications. Wenger then continues by pointing to recent strategies, breakthroughs and challenges in this field.

For precisely the above reasons, as one component of the entire and ongoing investigation, the present review compares DFT, electrochemical and spectral data of not only Ru [7] and Fe [8,9], but also other neighboring elements, namely Mn [10], Co [11,12] and Os [13]. In fact, the focus is on the theoretical prediction of redox potentials and absorbance spectra, as these are of primary importance in the development of photocatalysts, see Scheme 2 for relevant electro- and photochemical pathways. (All aspects henceforth mentioned and related to these five metals, are obtained from the above publications, without referencing again.)

Redox potentials can theoretically be predicted using several approaches:

- *Calculating absolute redox potential E*

Ccalculating the redox potential E from the free energy ΔG involved in the solvent phase redox reaction,

$$E(\text{absolute redox potential}) = \frac{-\Delta G_{\text{redox reaction}}}{nF}$$

using a free energy cycle as described and applied in literature [11,14–22], eg. Scheme 1.

- *Calculating Molecular Electrostatic Potential (MESP)*

* Corresponding author.
*E-mail addresses:* vEschwKG@ufs.ac.za (K.G. von Eschwege), ConradJ@ufs.ac.za (J. Conradie).
[1] ORCID: 0000-0002-8120-6830.
[2] ORCID: 0000-0001-8801-4703.

https://doi.org/10.1016/j.elecom.2022.107225

Available online 30 January 2022

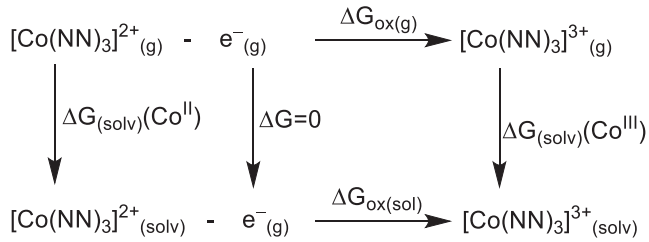


**Scheme 1.** Thermodynamic cycle for calculation of the absolute potential of Co $(NN)_3^{2+}$ oxidation. $\Delta G_{ox(g)}$ = free energy change in gas phase; $\Delta G_{(solv)}$ = solvation energy of gas phase species; $\Delta G_{ox(sol)}$ = change of free energy during oxidation reaction in solution [11]. NN = bidentate polypyridyl ligand. Reprinted from Inorganica Chimica Acta, 486, Hendrik Ferreira, Marrigje M. Conradie, Jeanet Conradie, Electrochemical and electronic properties of a series of substituted polypyridine ligands and their Co(II) complexes, 26-35, 2019, with permission from Elsevier.

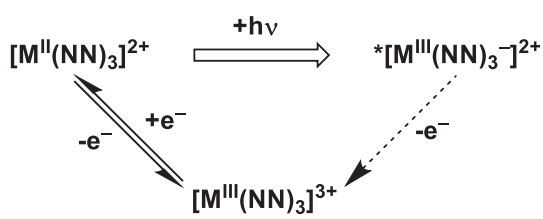


**Scheme 2.** Single electron photochemical excitation and redox reactions of MLCT polypyridyl complexes.

Using relationships between the different MESP properties of molecules with their experimental redox potentials [18,21–25].

- *From calculated electron affinities (EA) and ionization potentials (IP)*

Using relationships between calculated IP and oxidation potential or EA and reduction potential [7,13,26].

- *From calculated HOMO and LUMO energies*

It is well-known that highest occupied molecular orbital (HOMO) energies are related to oxidation potentials and lowest unoccupied molecular orbital (LUMO) energies are related to reduction potentials [27]. However, not many researchers used relationships between HOMO/LUMO energies and oxidation/reduction potentials to predict redox potentials. We previously demonstrated that these relationships can be used with unequalled simplicity and significant accuracy [7,10,13,28,29].

## 2. Syntheses

Scheme 3 shows the general methods used for complexation of the present row-4 and group-8 metals. Whereas the former (Mn, Fe & Co) are readily synthesized at room temperature, a much higher temperature of *ca* 200 °C is required during the complexation reactions of ruthenium and osmium. Both $Os^{III}$ and $Ru^{III}$ starting oxidation states had to be reduced to the $M^{II}$ state, as required by comparative cyclic voltammetry studies where oxidation electrochemical scans were initiated from the divalent complexed metals. The use of dipropylene glycol and ethylene glycol as solvents during the ruthenium and osmium complexation reactions simultaneously serve as mildly reducing agents, however requiring much longer reaction times. As indicated for ruthenium, strongly reducing ascorbic acid may be added to significantly reduce reaction time from eg. 16 h required for osmium, to 15 min for ruthenium. Yields are generally in excess of 60 %. If not using a metal

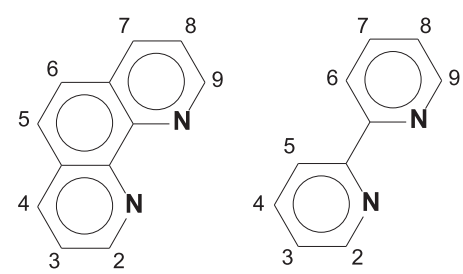


**Fig. 1.** Numbering scheme of 1,10-phenanthroline (phen, *left*) and bipyridyl (bpy, *right*) derivatives.

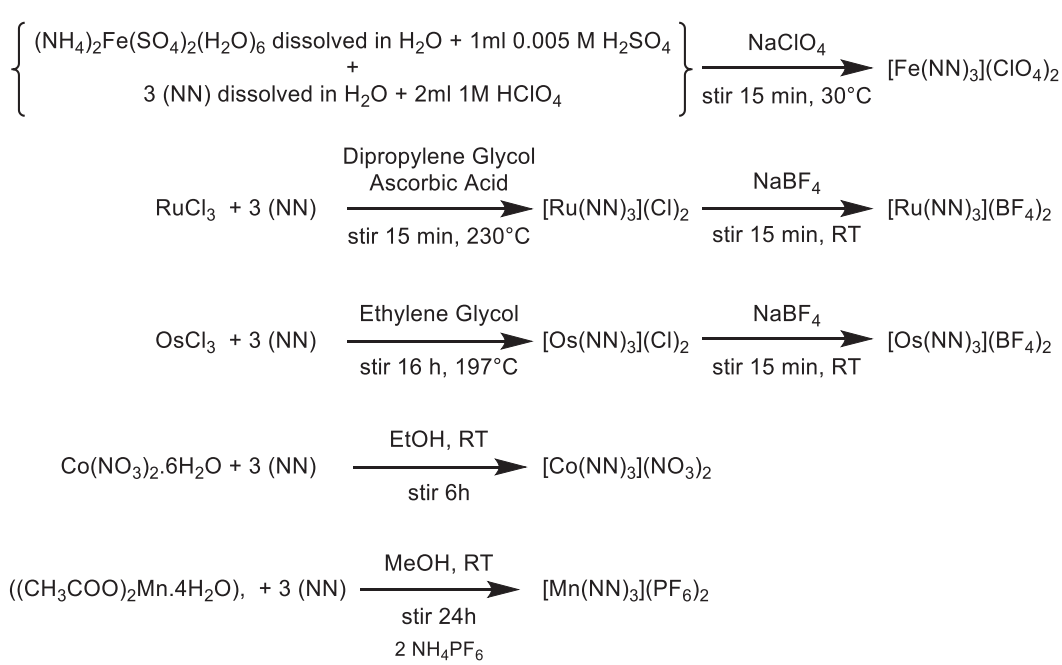


**Scheme 3.** Syntheses of Fe, Ru, Os, Mn & Co divalent MLCT polypyridyl complexes.

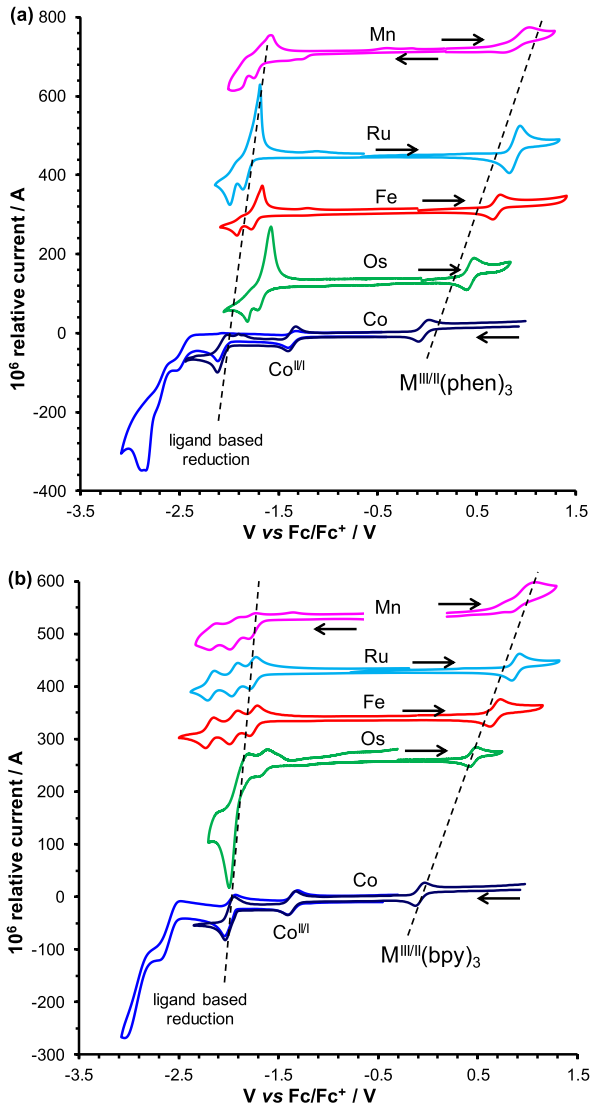


**Fig. 2.** Cyclic voltammograms of $[M(NN)_3]^{2+}$ where M = Mn, Ru, Fe, Os & Co. (a) NN = 1,10-phenanthroline and (b) NN = bipyridyl. All CV's were obtained (*vs* $Fc/Fc^+$) at a scan rate of 0.100 V $s^{-1}$ in 0.200 mol $dm^{-3}$ $TBAPF_6/CH_3CN$, on a glassy carbon working electrode at 20 °C. Scans were initiated in the direction indicated.

salt reagent with non-coordinating anion, a final synthesis step needs to be included, i.e. shortly refluxing the complex in the presence of an excess amount of salt containing the required non-coordinating anion. The absence of a strongly coordinating anion minimizes the effect of the cation in metal-based redox processes during electrochemical measurements.

In order to study closely related series of metal polypyridyl complexes with widely differing redox potentials, reported studies included ligands varying from $NH_2$–substituted electron-donating up to the strongly electron-withdrawing $NO_2$–substituted ligand derivatives. For the purpose of the present review only the following eight derivatives were used throughout all five previous studies and for comparative reasons considered here: phen, bpy, 5-Cl-phen, 4-Me-phen, 4,4′-Me-bpy, 4,4′-tBu-bpy, 3,4,7,8-Me-phen and 4,4′-OMe-bpy. The related substituent numbering scheme is shown in Fig. 1.

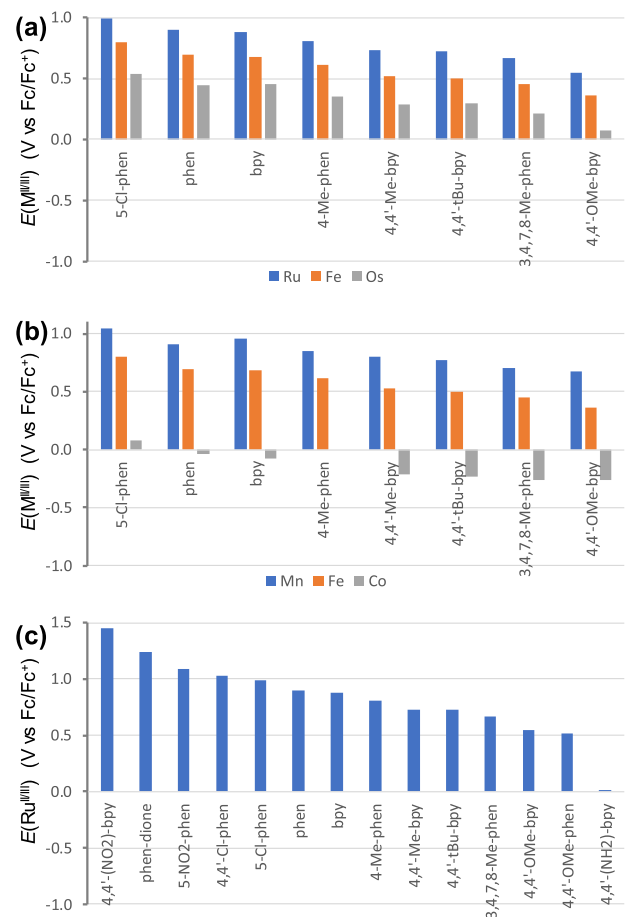


**Fig. 3.** Experimental $[M^{II/III}(polypyridyl)_3]$ oxidation potentials obtained at a scan rate of 0.100 V $s^{-1}$ in 0.200 mol $dm^{-3}$ $TBAPF_6/CH_3CN$, on a glassy carbon working electrode at 20 °C, of (a) Column-8 Fe, Ru & Os, and (b) Row-4 Mn, Fe & Co complex series involving differently substituted polypyridyl ligands. (c) Series of Ru complexes.

**Table 1**
$M^{II/III}$ reduction potentials (in V) for the bipyridine and phenanthroline metal complexes.

| | Experimental | | DFT (from $E_{HOMO}$) | | DFT (from $\chi_{Mull}$) | | DFT (from ω) | |
|---|---|---|---|---|---|---|---|---|
| Metal | $E^{o\prime}$ (bpy) | $E^{o\prime}$ (phen) | $E^{o\prime}$ (bpy) | $E^{o\prime}$ (phen) | $E^{o\prime}$ (bpy) | $E^{o\prime}$ (phen) | $E^{o\prime}$ (bpy) | $E^{o\prime}$ (phen) |
| Mn | 0.961[a] | 0.908[a] | 0.907 | 0.934 | 0.931 | 0.944 | 0.907 | 0.904 |
| Ru | 0.883 | 0.897 | 0.881 | 0.899 | 0.891 | 0.885 | 0.869 | 0.826 |
| Fe | 0.682 | 0.698 | 0.703 | 0.717 | 0.667 | 0.664 | 0.670 | 0.640 |
| Os | 0.452 | 0.444 | 0.443 | 0.453 | 0.420 | 0.408 | 0.431 | 0.387 |
| Co | −0.081 | −0.036 | −0.051 | 0.004 | −0.060 | −0.047 | −0.033 | −0.069 |
| average deviation (AD) | | | 0.023 | 0.019 | 0.021 | 0.026 | 0.030 | 0.044 |
| mean average deviation (MAD) | | | 0.015 | 0.011 | 0.008 | 0.011 | 0.017 | 0.021 |

a Mean of the peak oxidation and peak reduction potentials, $E_{1/2} = ½(E_{pa} + E_{pc})$

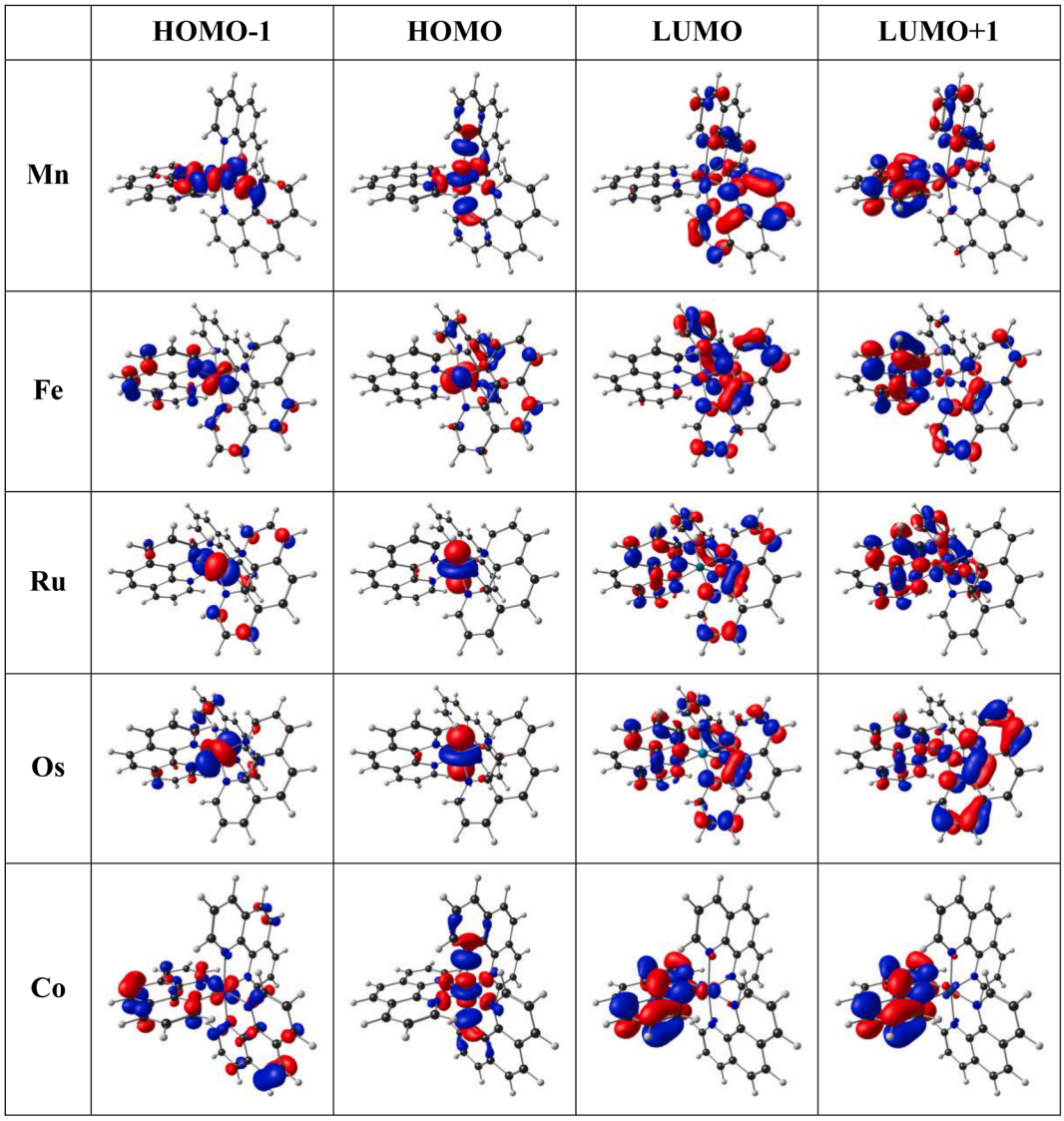


**Fig. 4.** Selected molecular orbital renderings for the metal(II)-1,10-phenanthroline complexes of Mn, Fe, Ru, Os & Co. An isosurface of 0.03 eÅ$^{-3}$ was used for the orbital plots.

## 3. Electrochemistry

Within the wide-scan cyclic voltammograms obtained in acetonitrile and tetrabutylammonium hexafluorophosphate ($TBAPF_6$) as electrolyte, all the metals showed a characteristic $M^{II/III}$ single oxidation peak, see Fig. 2. Of these, only the $Mn^{II/III}$ wave is irreversible, while $Co^{II/III}$, $Fe^{II/III}$, $Ru^{II/III}$ and $Os^{II/III}$ all are reversible. The most positive oxidation potential is found for the manganese bipyridyl complex (with $E_{1/2}$ = 0.961 V), while cobalt lies at the opposite end, with a negative $E^{o\prime}$ of −0.081 V, giving a difference of 1.042 V, see Table 1. Interestingly, the corresponding range is contracted by 0.098 V in the phenanthroline complexes. Cobalt is the only metal that also shows a second metal-centered redox couple, namely that of $Co^{I/II}$, at −1.37 V. All remaining low-voltage redox waves are ascribed to ligand-based reductions, with iron and ruthenium being most similar in this region. The first ligand-based reduction potentials of the iron complexes occur at −1.784 (bpy), −1.768 (phen) and −1.685 V (tpy) (tpy = terpyridine) respectively. Corresponding values for ruthenium are in the same region, i.e. −1.754 (bpy) and −1.774 V (phen).

The above-mentioned values are related to only the unsubstituted species. The bar diagrams in Fig. 3 a - c clearly illustrates the effect of substituting the polypyridyl ligands with groups that vary with regard to electronegativity. The comparisons combine $E(M^{II/III})$ of both the bipyridine and phenanthroline complex series, consisting of the eight derivatives that were likewise involved in all five metals of this discussion. As is expected, the electron-withdrawing substituent, Cl, instills greatest resistance to oxidation, while the electron-donating substituent, OMe, drives $E(M^{II/III})$ to the opposite end, allowing for much easier oxidations to occur. This trend is similar for all five metals. Relative to the redox couple of ferrocene ($Fc/Fc^+$), cobalt is the only metal with negative oxidation potentials in all but one, 5-Cl-phenanthroline cobalt (II), ranging from −0.27 V to 0.08 V *vs* $Fc/Fc^+$. The implication of the more negative redox couples in the $[Co^{II/III}(polypyridyl)_3]$ series is that these complexes could be used to replace the commonly used iodide/triiodide ($I_3^-/I^-$) redox mediator in dye-sensitized solar cells, DSSC. The redox potential of the ($I_3^-/I^-$) redox couple is −0.34 ± 0.02 V *vs* $Fc/Fc^+$ in acetonitrile [30]. Alternative redox mediators may have redox potentials up to 0.5 V more positive than that of iodide/triiodide [31], i.e. redox potentials in the range −0.34 V to 0.24 V *vs* $Fc/Fc^+$. It should be noted that the choice of a successful mediator in a specific DSSC also depends on the electronic properties of the specific dye in that cell [32].

Overall, the redox range for the full series of each metal varies over almost 0.5 V. Complexes containing the stronger electron-withdrawing $NO_2$ and the strong electron-donating $NH_2$ substituent group, which

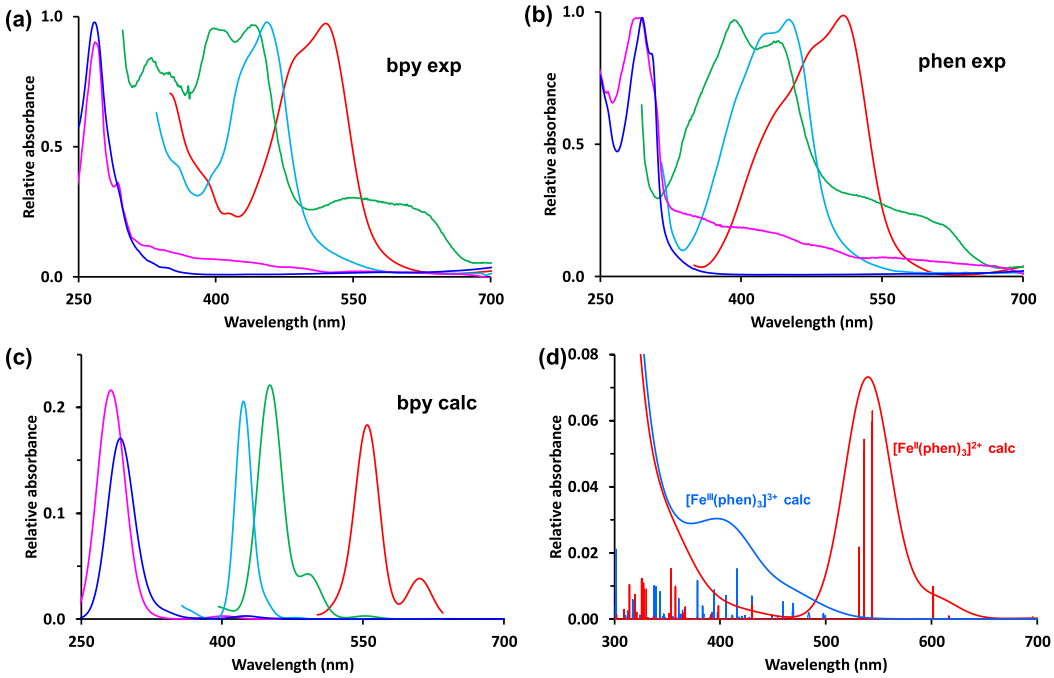


**Fig. 5.** (a) and (b): Experimental UV–visible spectra showing the MLCT-band from solvents methanol (Fe & Co), $CH_3CN$ (Mn) and DMSO (Ru & Os) for: (a) $[M(bpy)_3]^{2+}$ and (b) $[M(phen)_3]^{2+}$ complexes. (c) B3LYP gas phase TDDFT Gaussian broadening curves (30 nm halfwidth) of $[M(bpy)_3]^{2+}$ complexes, BP86/TZP TDDFT was used for Fe. (d): BP86/TZP gas phase TDDFT for $[Fe^{II}(phen)_3]^{2+}$ (red) and $[Fe^{III}(phen)_3]^{3+}$ (blue). Color code (a – c): $Mn^{II}$ – magenta, $Fe^{II}$ – red, $Co^{II}$ – dark blue, $Os^{II}$ – green, $Ru^{II}$ – light blue. (For interpretation of the references to color in this figure legend, the reader is referred to the web version of this article.)

did not feature in all the studies, increase the range significantly, to eg. almost 1.5 V, as reported for the $Ru^{II/III}$ redox couple, see Fig. 3 c.

## 4. Quantum chemistry

All density functional theory (DFT) computed results presented here were performed as described in our previous publications, using the B3LYP functional, except where otherwise indicated. Default criteria for geometry convergence (the root mean square force, the maximum force, the root mean square displacement and the maximum displacement within the threshold of 0.0 0 030, 0.0 0 045, 0.0 012 and 0.0 018 atomic units, respectively) and 1.0D-8 atomic unit for convergence on energy, were used as implemented in the Gaussian 16 package [33].

### 4.1. Molecular orbitals

Molecules which exhibit charge density shifts between molecular orbitals (MOs) that are predominantly located on the metal and MOs that are predominantly located on the ligand(s), are termed metal-to-ligand charge transfer complexes. The unsaturated heterocycles, bipyridine and phenanthroline, often have pronounced charge-transfer bands. Of these, $Ru(bpy)_3^{2+}$ is most well-known, with a long-lived photochemical excited state best described as $*[Ru^{III}(bipy^{-})(bipy)_2]^{2+}$ [2,34]. During photo-excitation an electron in the metal-located HOMO gets promoted to the LUMO on the ligand(s), without change in overall oxidation state. Electro-reduction is partly similar, i.e. with an electron being added to the LUMO, however without loss of the HOMO electron and thus change in oxidation state. Oxidation, on the other hand, implies the loss of a HOMO electron(s).

DFT computed molecular orbital renderings provide helpful insights with regard to the presence or absence of directional charge transfer capabilities of molecules. Fig. 4 shows orbital renderings of the phenanthroline coordinated species of all five metals. For Ru and Os more than 80% of the HOMOs are centered on the central metal, while Mn, Fe and Co also show metal-centered HOMOs, however with more than 33% of the HOMO spreading to the ligands. HOMO-1 is also mostly metal-centered for all 5 complexes. Both LUMO and LUMO + 1 are located on one or more of the ligands in all the complexes.

### 4.2. UV–visible spectra

Fig. 5 shows the experimental UV–vis spectra of the five metal complexes, for both ligands. When comparing bipyridine (5a) to phenanthroline (5b) complexes, relative absorbance peak shifts are minimal. However, when comparing the five different metals, a significant red-shift is seen towards Fe, and blue-shift towards Mn and Co. In fact, $\lambda_{max}$ for Mn and Co (for both bpy & phen) lies far into the UV region, i.e. at *ca* 270–300 nm, which renders these metal complexes useless in terms of solar photocatalytic commercial applications. Irradiation from the sun peaks just below 500 nm. If these metals are to be used as such, other means have to be pursued to affect the necessary red-shift. $\lambda_{max}$ for Fe $(phen)_3$/methanol lies at 509 nm, $Ru(phen)_3$/DMSO at 450 nm and Os $(phen)_3$/DMSO at 392 nm, however the osmium complexes also have peaks of slightly lower intensity at *ca* 440 nm and a broad shoulder spanning almost the entire visible region up to *ca* 650 nm.

Theoretical UV–visible region (250–700 nm) electronic oscillators were computed using time dependent DFT (TDDFT) in gas phase. It should be noted that TDDFT calculations with use of solvent, as opposed to gas phase, often results in better agreement with experiment. Particular functionals that are used for TDDFT calculations also affect spectral appearances. Fig. 5 (c) compares the simulated spectra, using Gaussian broadening curves, of the bipyridyl complexes of the five metals in the divalent state. The experimental trend for the MLCT band (red-shift for Fe and blue-shift for Mn and Co) is reproduced by the TDDFT calculations. $Fe(phen)_3$, as well-known redox indicator, changing color from red to blue upon oxidation [35], exhibits a blue-shift upon oxidation from $Fe^{II}$ to $Fe^{III}$, which is clearly in agreement with experiment [36], see Fig. 5 (d).

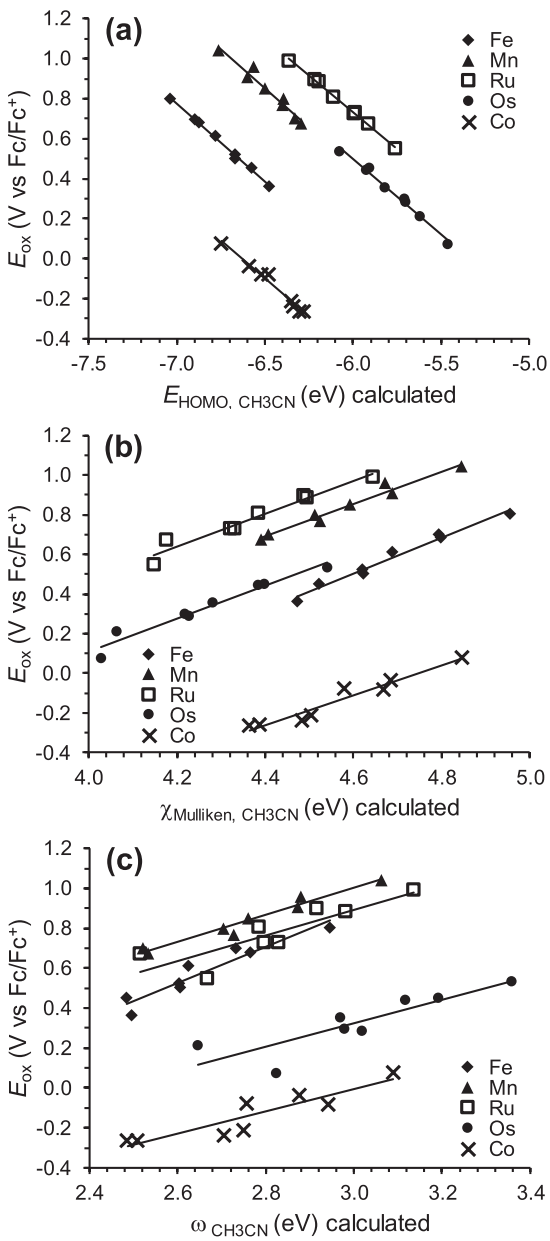


**Fig. 7.** Experimental oxidation potentials, $E_{ox}$ ($M^{II/III}$ *vs* $Fc/Fc^+$), of the five metal polypyridine series correlated with $CH_3CN$-phase computed (a) $E_{HOMO}$, (b) $\chi_{Mulliken}$, and (c) the global electrophilicity index (ω).

### 4.3. Correlations

Computed and experimental CV data from studies of the five metal complexes were extracted and evaluated for best correlations. Fig. 7a – c show plots of the $M^{II/III}$ experimental oxidation potentials *versus* DFT computed descriptors; $E_{HOMO}$, the Mulliken electronegativity ($\chi_{Mulliken}$) and global electrophilicity index (ω). A clear direct relationship is seen in all cases, for which corresponding linear equations ($y = mx + c$) are listed in Table 2. The goodness-of fit or coefficient of determination $R^2$ values related to the data series of each metal are also shown.

Correlating HOMO energies ($E_{HOMO}$) with experimental oxidation potentials, $E_{ox}$, clearly gives superior fits compared to any other computed descriptor that are considered here; $R^2$ values all are very close to unity, with Mn the lowest, i.e. at 0.95. Contrary to other quantities such as adiabatic IP, calculated redox and MESP potentials, which require additional calculations, HOMO energies are available directly from DFT geometry optimization output files, which makes it a most convenient parameter to utilize towards highly accurate theoretical prediction of redox potentials. Of course, for these theoretical calculations the gradient (m) and *y*-axis intercept (c) for each particular class of compounds should be available, which is indeed what is now supplied here, i.e. in Table 2. Interestingly, both the bipyridine and phenanthroline complexes of each metal linearly fit on the same straight line, however, when the central metals are changed, the major difference comes at the relative *y*-axes intercepts of trendlines. The gradients (m) of the various metal complexes are rather similar, nearing the ideal slope of −1 [12], with overall variation of m being only 0.05 in the correlation of $E_{ox}$ with $E_{HOMO}$.

**Table 2**
Linear relationships ($y = mx + c$) between experimental formal reduction potentials (*y*-axes) and DFT-computed descriptors (*x*-axes), related to Fig. 7a-c.

| DFT Descriptors | Complex M | $y = mx + c$ | $R^2$ |
|---|---|---|---|
| a. HOMO Energy ($E_{HOMO}$) | Fe | $E_{ox} = -0.79E_{HOMO} - 4.73$ | 1.00 |
| | Mn | $E_{ox} = -0.79E_{HOMO} - 4.28$ | 0.95 |
| | Ru | $E_{ox} = -0.74E_{HOMO} - 3.70$ | 1.00 |
| | Os | $E_{ox} = -0.76E_{HOMO} - 4.05$ | 0.99 |
| | Co | $E_{ox} = -0.77E_{HOMO} - 5.07$ | 0.98 |
| b. Mulliken Electronegativiy ($\chi_{Mulliken}$) | Fe | $E_{ox} = 0.90\chi_{Mul} - 3.65$ | 0.98 |
| | Mn | $E_{ox} = 0.82\chi_{Mul} - 2.90$ | 0.97 |
| | Ru | $E_{ox} = 0.83\chi_{Mul} - 2.84$ | 0.95 |
| | Os | $E_{ox} = 0.83\chi_{Mul} - 3.23$ | 0.95 |
| | Co | $E_{ox} = 0.75\chi_{Mul} - 3.56$ | 0.95 |
| c. Global Electrophilicity Index (ω) | Fe | $E_{ox} = 0.90\omega - 1.82$ | 0.90 |
| | Mn | $E_{ox} = 0.68\ \omega - 1.05$ | 0.96 |
| | Ru | $E_{ox} = 0.64\ \omega - 1.04$ | 0.75 |
| | Os | $E_{ox} = 0.58\ \omega - 1.42$ | 0.75 |
| | Co | $E_{ox} = 0.56\ \omega - 1.68$ | 0.83 |

To illustrate the accuracy of this approach, theoretically calculated oxidation potentials using the equations in Table 2 are also included in Table 1. As an example, the experimental $E_{ox}$ value of the $Ru^{II}(phen)_3$ complex was measured as 0.897 V. Using the DFT calculated acetonitrile-phase $E_{HOMO}$ value of −6.214 eV in the equation, $E_{ox} = -0.74E_{HOMO} - 3.70$, gives the corresponding theoretically predicted value of 0.899 V, i.e. a difference of merely 0.002 V, which lies well within experimental error of measured redox potentials. A maximum deviation of 0.07 V for calculated values in Table 1 was found, while the maximum average deviation is 0.04 V. The maximum mean average deviation (MAD) value, a measure of the variability in a data set, is only 0.02 V, showing that DFT (equations in Table 2 obtained from relationships in Fig. 7a-c) can be used for the theoretical prediction of redox potentials.

## 5. Conclusion

The neighbouring polypyridyl complexes of row-4; Mn, Fe & Co, and of column-8; Fe, Ru & Os, are readily synthesized with yields in excess of 60 %. All these complexes exhibit metal-to-ligand charge transfer according to molecular orbital renderings, which is most clearly the case for the Ru and Os compounds. Experimental redox data correlate very closely with HOMO energies of each type of metal complex. The linear equations hereby established, provide a means of predicting oxidation potentials of related compounds, of which HOMO energies may be calculated by means of DFT/B3LYP.

## Declaration of Competing Interest

The authors declare that they have no known competing financial

interests or personal relationships that could have appeared to influence the work reported in this paper.

## Acknowledgements

This work received support from the South African National Research Foundation (grant numbers 129270 and 132504). The High-Performance Computing facility of the UFS, the CHPC of South Africa and the Norwegian Supercomputing Program (UNINETT Sigma2, Grant No. NN9684K) are acknowledged for computer time.

## References

[1] H.B. Gray, Powering the planet with solar fuel, Nat. Chem. 1 (2009) 7–7. doi: 10.1038/nchem.141.
[2] O.S. Wenger, Is Iron the New Ruthenium? Chem. – A Eur. J. 25 (24) (2019) 6043–6052, https://doi.org/10.1002/chem.201806148.
[3] I. Benesperi, H. Michaels, M. Freitag, The researcher's guide to solid-state dye-sensitized solar cells, J. Mater. Chem. C. 6 (44) (2018) 11903–11942, https://doi.org/10.1039/C8TC03542C.
[4] S. Aghazada, M. Nazeeruddin, Ruthenium Complexes as Sensitizers in Dye-Sensitized Solar Cells, Inorganics. 6 (2018) 52, https://doi.org/10.3390/inorganics6020052.
[5] N.W. Kinzel, C. Werlé, W. Leitner, Transition Metal Complexes as Catalysts for the Electroconversion of $CO_2$: An Organometallic Perspective, Angew. Chemie Int. Ed. 60 (2021) 11628–11686, https://doi.org/10.1002/anie.202006988.
[6] J. Guerra, D. Cantillo, C.O. Kappe, Visible-light photoredox catalysis using a macromolecular ruthenium complex: reactivity and recovery by size-exclusion nanofiltration in continuous flow, Catal, Sci. Technol. 6 (13) (2016) 4695–4699, https://doi.org/10.1039/C6CY00070C.
[7] D. van der Westhuizen, K.G. von Eschwege, J. Conradie, Electrochemistry and spectroscopy of substituted $[Ru(phen)_3]^{2+}$ and $[Ru(bpy)_3]^{2+}$ complexes, Electrochim. Acta. 320 (2019) 134540, https://doi.org/10.1016/j.electacta.2019.07.051.
[8] H. Ferreira, K.G. von Eschwege, J. Conradie, Electronic properties of Fe charge transfer complexes – A combined experimental and theoretical approach, Electrochim. Acta. 216 (2016) 339–346, https://doi.org/10.1016/j.electacta.2016.09.034.
[9] K.G. von Eschwege, J. Conradie, Iron phenanthrolines: A density functional theory study, Inorganica Chim. Acta. 471 (2018) 391–396, https://doi.org/10.1016/j.ica.2017.11.047.
[10] Z. Mtshali, K.G. von Eschwege, J. Conradie, Electrochemical study of the Mn(II/III) oxidation of tris(polypyridine)manganese(II) complexes, Electrochim. Acta. 391 (2021) 138965, https://doi.org/10.1016/j.electacta.2021.138965.
[11] H. Ferreira, M.M. Conradie, J. Conradie, Electrochemical and electronic properties of a series of substituted polypyridine ligands and their Co(II) complexes, Inorganica Chim. Acta. 486 (2019) 26–35, https://doi.org/10.1016/j.ica.2018.10.020.
[12] H. Ferreira, M.M. Conradie, J. Conradie, Electrochemical properties of a series of Co(II) complexes, containing substituted phenanthrolines, Electrochim. Acta. 292 (2018) 489–501, https://doi.org/10.1016/j.electacta.2018.09.151.
[13] D. Westhuizen, J. Conradie, K.G. Eschwege, Electrochemistry of Os Bipyridyl and Phenanthroline Complexes, Comparison with Ru and Fe, Electroanalysis. 32 (12) (2020) 2838–2851, https://doi.org/10.1002/elan.202060300.
[14] A. Lewis, J.A. Bumpus, D.G. Truhlar, C.J. Cramer, Molecular Modeling of Environmentally Important Processes: Reduction Potentials, J. Chem. Educ. 81 (2004) 596–604, https://doi.org/10.1021/ed081p596.
[15] A.V. Marenich, J. Ho, M.L. Coote, C.J. Cramer, D.G. Truhlar, Computational electrochemistry: Prediction of liquid-phase reduction potentials, Phys. Chem. Chem. Phys. 16 (29) (2014) 15068–15106, https://doi.org/10.1039/C4CP01572J.
[16] M.H. Baik, R.A. Friesner, Computing redox potentials in solution: Density functional theory as a tool for rational design of redox agents, J. Phys. Chem. A. 106 (2002) 7407–7412, https://doi.org/10.1021/jp025853n.
[17] H. Vázquez-Lima, P. Guadarrama, Analysis of structural factors related to spectroscopic data and redox potentials of CuT1 models through DFT tools, Int. J. Quantum Chem. 112 (5) (2012) 1431–1438, https://doi.org/10.1002/qua.23130.
[18] A.A. Adeniyi, J. Conradie, Electronic effect of β-diketonato ligands on the redox potential of fac and mer tris(β-diketonato) iron(III) complexes: A density functional theory study and molecular electrostatic potential analysis, Int. J. Quantum Chem. e26036 (2019) 1–14.
[19] A.A. Adeniyi, J. Conradie, Influence of substituents on the reduction potential and $pK_a$ values of β-diketones tautomers: A theoretical study, Electrochim. Acta. 297 (2019) 947–960, https://doi.org/10.1016/j.electacta.2018.12.030.
[20] A.A. Adeniyi, J. Conradie, Computational insight into the contribution of para-substituents on the reduction potential, proton affinity, and electronic properties of nitrobenzene compounds, J. Mol. Model. 25 (2019) 78, https://doi.org/10.1007/s00894-019-3946-2.
[21] A.A. Adeniyi, J. Conradie, Substituent and isomeric effects on the reduction and oxidation potential of tris(β -diketonato) manganese(III) complexes : DFT and MESP analysis, South African J. Sci. Technol. 38 (2019) 728. doi:http://www.satnt.ac.za/index.php/satnt/ article/view/728.
[22] A.A. Adeniyi, M. Landman, J. Conradie, Mo Fischer Carbene Complexes: A DFT Study on the Prediction of Redox Potentials, J. Electrochem. Soc. 168 (6) (2021) 066523, https://doi.org/10.1149/1945-7111/ac0a28.
[23] B.A. Anjali, F.B. Sayyed, C.H. Suresh, Correlation and Prediction of Redox Potentials of Hydrogen Evolution Mononuclear Cobalt Catalysts via Molecular Electrostatic Potential: A DFT Study, J. Phys. Chem. A. 120 (7) (2016) 1112–1119, https://doi.org/10.1021/acs.jpca.5b11543.
[24] B.A. Anjali, C.H. Suresh, Electronic effect of ligands vs. reduction potentials of Fischer carbene complexes of chromium: a molecular electrostatic potential analysis, New J. Chem. 42 (22) (2018) 18217–18224, https://doi.org/10.1039/C8NJ04184A.
[25] J. Conradie, Redox behaviour of $[Ru(\beta\text{-diketonato})_3]$ compounds, Electrochim. Acta. 337 (2020) 135801, https://doi.org/10.1016/j.electacta.2020.135801.
[26] R.S. Ruoff, K.M. Kadish, P. Boulas, E.C.M. Chen, Relationship between the Electron Affinities and Half-Wave Reduction Potentials of Fullerenes, Aromatic Hydrocarbons, and Metal Complexes, J. Phys. Chem. 99 (21) (1995) 8843–8850, https://doi.org/10.1021/j100021a060.
[27] J. Conradie, A Frontier orbital energy approach to redox potentials, J. Phys. Conf. Ser. 633 (2015) 012045, https://doi.org/10.1088/1742-6596/633/1/012045.
[28] A. Kuhn, K.G. von Eschwege, J. Conradie, Reduction potentials of para-substituted nitrobenzenes-an infrared, nuclear magnetic resonance, and density functional theory study, J. Phys. Org. Chem. 25 (1) (2012) 58–68, https://doi.org/10.1002/poc.1868.
[29] K.G. von Eschwege, J. Conradie, Redox Potentials of Ligands and Complexes – a DFT Approach, S. Afr. J. Chem. 64 (2011) 203–209. https://hdl.handle.net/10520/EJC24537.
[30] X. Wang, D.M. Stanbury, Oxidation of Iodide by a Series of Fe(III) Complexes in Acetonitrile, Inorg. Chem. 45 (8) (2006) 3415–3423, https://doi.org/10.1021/ic052022y10.1021/ic052022y.s001.
[31] G. Boschloo, A. Hagfeldt, Characteristics of the iodide/triiodide redox mediator in dye-sensitized solar cells, Acc. Chem. Res. 42 (11) (2009) 1819–1826, https://doi.org/10.1021/ar900138m.
[32] J. Conradie, Polypyridyl copper complexes as dye sensitizer and redox mediator for dye-sensitized solar cells, Electrochem. Commun. 134 (2022) 107182, https://doi.org/10.1016/j.elecom.2021.107182.
[33] M.J. Frisch, G.W. Trucks, H.B. Schlegel, G.E. Scuseria, M.A. Robb, J.R. Cheeseman, G. Scalmani, V. Barone, G.A. Petersson, H. Nakatsuji, X. Li, M. Caricato, A. V. Marenich, J. Bloino, B.G. Janesko, R. Gomperts, B. Mennucci, H.P. Hratchian, J. V. Ortiz, A.F. Izmaylov, J.L. Sonnenberg, D. Williams-Young, F. Ding, F. Lipparini, F. Egidi, J. Goings, B. Peng, A. Petrone, T. Henderson, D. Ranasinghe, V.G. Zakrzewski, J. Gao, N. Rega, G. Zheng, W. Liang, M. Hada, M. Ehara, K. Toyota, R. Fukuda, J. Hasegawa, M. Ishida, T. Nakajima, Y. Honda, O. Kitao, H. Nakai, T. Vreven, K. Throssell, J. Montgomery, J. A., J.E. Peralta, F. Ogliaro, M.J. Bearpark, J.J. Heyd, E.N. Brothers, K.N. Kudin, V.N. Staroverov, T.A. Keith, R. Kobayashi, J. Normand, K. Raghavachari, A.P. Rendell, J.C. Burant, S.S. Iyengar, J. Tomasi, M. Cossi, J.M. Millam, M. Klene, C. Adamo, R. Cammi, J.W. Ochterski, R.L. Martin, K. Morokuma, O. Farkas, J.B. Foresman, D.J. Fox, Gaussian 16, Revision B.01, (2016).
[34] K. Kalyanasundaram, Photochemistry of polypyridine and porphyrin complexes, Academic Press, London, 1992.
[35] I.M. Kolthoff, V.A. Stenger, Volumetric Analysis, Interscience, New York, 1942.
[36] L. Kozak, P. Niedzielski, W. Wachowiak, The tandem analytical method of flow injection diode array spectrophotometry and flame atomic absorption spectrometry (FI-DAD(vis)-FAAS) in iron speciation studies using 1,10-phenanthroline complexes, Microchem. J. 110 (2013) 54–60, https://doi.org/10.1016/j.microc.2013.02.004.